Positron scattering from pyrimidine

P. Palihawadana,[1] R. Boadle,[1] L. Chiari,[2] E. K. Anderson,[1] J. R. Machacek,[1] M. J. Brunger,[2,3]
S. J. Buckman,[1,3] and J. P. Sullivan[1]

[1]*ARC Centre for Antimatter-Matter Studies, Research School of Physics and Engineering, Australian National University, Canberra 0200, Australia*

[2]*ARC Centre for Antimatter-Matter Studies, School of Chemical and Physical Sciences, Flinders University, GPO Box 2100, Adelaide 5001, Australia*

[3]*Institute of Mathematical Sciences, University of Malaya, Kuala Lumpur, Malaysia*

(Received 17 May 2013; published 31 July 2013)

In the present work we report on our experimental total cross section and positronium formation cross-section results for positron scattering from pyrimidine for energies from 1 to 180 eV. In addition, the total inelastic integral cross sections (for electronic excitations plus direct ionization) have been measured up to 21.5 eV. We also report quasi-elastic total and differential cross sections at energies up to 21.5 eV. Our results are compared to recent theoretical and experimental data for positron scattering, as well as recent work on electron scattering from this target.

DOI: 10.1103/PhysRevA.88.012717 PACS number(s): 34.80.Bm, 34.80.Uv, 34.80.Lx, 34.80.Gs

I. INTRODUCTION

Positron interactions with biologically relevant molecules have recently gained considerable interest, both experimentally and theoretically, among atomic and molecular physics and medical science communities [1]. This has been driven partly by the increasing use of positrons in modern medical diagnostic and treatment procedures, such as positron emission tomography (PET) scans, positherapy, and other applications of fluorodeoxyglucose (FDG) for therapy [2]. It is important to understand and account for the radiation damage caused by positrons in the process of thermalization within the biological medium [1]. In addition, the use of cross sections and energy loss data to incorporate the effects of low-energy electrons and positrons in radiation interaction models has received increased interest in recent years [1,3,4]. It is hoped this will lead to a better physical picture of the particle track which could be supplementary to more established Monte Carlo-based codes, such as PENELOPE [5] and GEANT4 [6].

Although there are some similarities between the two processes, the mechanisms leading to biological damage are qualitatively and quantitatively different for positrons and electrons [7]. For example, the unique positronium (Ps) formation channel in positron interactions, which generates gamma rays while annihilating inside the biological medium, could increase the ionizing effect inside the organic tissue [7]. While there are many unanswered questions about the interactions of positrons with biomolecules [8], there has been very little experimental or theoretical work done in the past to understand and quantify positron interactions with biological systems, hence our knowledge about processes that take place at the atomic and molecular level remains poor. This work is part of a broader study to investigate positron interactions with biologically important molecules, such as water and formic acid [9], tetrahydrofuran (THF) [10], and 3-hydroxy-tetrahydrofuran (3-hTHF) [11].

Here we present a detailed study of positron interactions with pyrimidine. Pyrimidine ($C_4H_4N_2$) is a heterocyclic aromatic organic compound containing two nitrogen atoms at positions 1 and 3 of the six-member ring. It is considered as a model molecule to investigate electron and positron interactions with DNA and RNA bases [12] due to the similarity of its ring structure to three of the five nucleobases, namely, cytosine ($C_4H_5N_3O$), thymine ($C_5H_6N_2O_2$), and uracil ($C_4H_4N_2O_2$), which are pyrimidine derivatives. Pyrimidine also possesses some interesting physico-chemical properties which make it an appealing molecule to study from a fundamental perspective. These include an isotropic dipole polarizability (α) of $\sim$59.3 a.u. [13] and a relatively large permanent dipole moment (μ) of $\sim$2.33 D [14]. As we have seen in our previous studies, for both positrons (e.g., [9,10]) and electrons (e.g., [15,16]), such target molecular properties can have an important impact on the scattering dynamics of the system under study. This point will be revisited later in our discussion.

To the best of our knowledge there has been only one previous study on positron scattering from pyrimidine by Zecca *et al*. [17]. They reported total cross sections (TCS) for positron scattering from pyrimidine, along with theoretical TCS for the corresponding electron scattering calculated using the independent atom model with screened additivity rule (IAM-SCAR) correction. In this work, we compare those TCS results by Zecca *et al*. with the present experimental measurements, along with recently developed theoretical calculations for positron scattering using the IAM-SCAR and *R*-matrix formalisms [18]. We have also compared our positron differential cross-section results to some recent electron scattering measurements. Recently Palihawadana *et al*. [15] reported absolute elastic differential and integral cross sections and elastic excitation function measurements for low-energy electron scattering from pyrimidine, together with theoretical cross sections calculated using the *ab initio* Schwinger multichannel variational technique (SMC) and the IAM-SCAR model. These DCS results are compared directly with the present positron scattering DCS measurements in the results and discussion section.

II. EXPERIMENTAL DETAILS

An experimental apparatus at the Australian National University, based on the Surko trap system [19], was used to take the measurements presented here. A detailed description

of the experimental setup has been given previously [20] so that only a brief overview of the operation is given here. A radioactive ^{22}Na isotope with activity ∼40 mCi was used to obtain the positrons for this work. High-energy positrons emitted from the source are moderated using a solid Ne moderator to form a low-energy positron beam with a measured beam width of ∼1.5 eV. The moderated positron beam is confined using a solenoidal magnetic field (∼100 G) and transported into a two-stage Surko trap in a stronger (∼530 G), uniform magnetic field. The trap electrodes form a stepped electrostatic potential well, resulting in the positrons losing energy and becoming trapped via inelastic collisions with a mixture of N_2 and CF_4 buffer gases. The positrons thermalize to gas (room) temperature due to further collisions. The resulting cloud of positrons becomes the reservoir for the pulsed positron beam used in this work. The trap operation is cycled at approximately 100–200 Hz with up to 1000 positrons emitted per pulse, with an energy width between 40–60 meV for the experiments discussed here.

The pulsed positron beam is directed into a scattering cell made of gold-plated copper, with length 50 mm and entrance and exit apertures of 5-mm diameter. The potential of the scattering cell defines the energy of the positrons within the cell. The target density inside the cell is maintained such that the number of scattering events is less than or equal to 10% of the unscattered beam intensity to minimize multiple scattering effects. After transit through the cell, the beam passes through a retarding potential analyzer (RPA) which is sensitive only to the parallel energy component, or $E_{||}$, of the beam. The positrons transmitted by the RPA are finally detected by a microchannel plate detector assembly and recorded by the experimental control computer.

The analysis used for this experiment has been explained in detail in a number of publications [10,21], and relies on the analysis of the parallel energy component ($E_{||}$) of the scattered beam. Angular scattering results in a loss of $E_{||}$, which can then be related to the differential scattering cross section. If the total energy loss is also possible (i.e., above the first inelastic threshold), then this can be separated out by changing the magnetic field at the RPA, relative to the scattering cell. Positronium formation appears as a loss in the primary beam current. The resolution of inelastic events relies on the energy resolution of the positron beam, as well as the maximum magnetic field ratio possible (between the scattering cell and RPA). In these experiments, with a field ratio of 5, vibrational and rotational scattering are unable to be distinguished from elastic scattering. Electronic excitation and ionization can be isolated from the elastic component, although not from each other. As a result, the measurements presented here are of the grand total cross section, positronium formation cross section, quasi-elastic scattering, and total inelastic (electronic excitation and ionisation) scattering. It should be noted that at most energies studied, the contribution of rotational and vibrational excitation is likely to be small. The absolute calibration of the cross section is given simply by the length of the gas cell and the pressure of the gas, and all cross-section values presented in this paper are absolute. Experimental errors arise from the accuracy of the measurement of these parameters, as well as the statistical quality of the data, and thus absolute total errors are provided for the present data.

TABLE I. Missing forward angles for grand total and total elastic cross sections presented in this work.

Energy [eV]	θ_C (GTCS)	θ_C (elastic)
2	11	26
5	7	16
10	5	13
20	3	8
50	2	–
100	1.5	–
180	1	–

Due to the magnetic field confinement, our energy resolution provides the limit on the angular resolution of the measurements. In particular, in the case of the grand total and total elastic cross sections, some of the forward angle scattering is unable to be distinguished from the primary unscattered beam. This leads to an underestimation of the cross section in each case, as has been outlined by Sullivan *et al.* [22]. In the case of a polar target, in particular at low energies where the angular resolution is poorest, the measured cross section can be significantly lower than the true total cross section, as was demonstrated in the case of positron scattering from water [9]. For the present experiments, our minimum measurable angle of scattering (θ_C) is shown for selected energies in Table I, and must be kept in mind when making any comparison to other data.

A high-purity (99% or better) liquid sample of pyrimidine from Sigma-Aldrich was used to generate the pyrimidine vapor. At room temperature, the vapor pressure above the liquid pyrimidine sample was around 12 Torr which, via a needle valve, was sufficient to provide the gas pressure of 0.09 to 0.3 mTorr used in the cell to achieve the required beam attenuation. The pyrimidine sample was also degassed, using several freeze-pump-thaw cycles, under a vacuum, before taking the measurements. This was done to minimize any possible impurities in the source. In the present work, the temperature of the gas lines and valve(s) that controlled the flow of gas were kept at around 50 °C to help prevent the condensation of pyrimidine vapor on the inner walls of the gas lines and valve(s) [15]. The pressure gauge used to measure the scattering cell target pressure is a model 690 MKS Baratron capacitance manometer with a full range of 1 torr and a measurement accuracy of about 5% for the low-pressure range that was used for these measurements.

III. RESULTS AND DISCUSSION

A. Grand total cross section

In Fig. 1, our present experimental data are shown in comparison to the previous data from the Trento group [17], along with the IAM-SCAR calculations of Sanz *et al.*, which include rotational contributions [18]. Also presented are the theoretical calculations excluding the missing angles of the experiment, as described above. The present cross section is larger than that of Zecca *et al.* at all energies, which is consistent with previous comparisons of the data between the two experimental groups (for example, see [9]), and mostly due to differences in the angular resolution of the two experiments, combined with the forward peaked nature of the differential cross section that

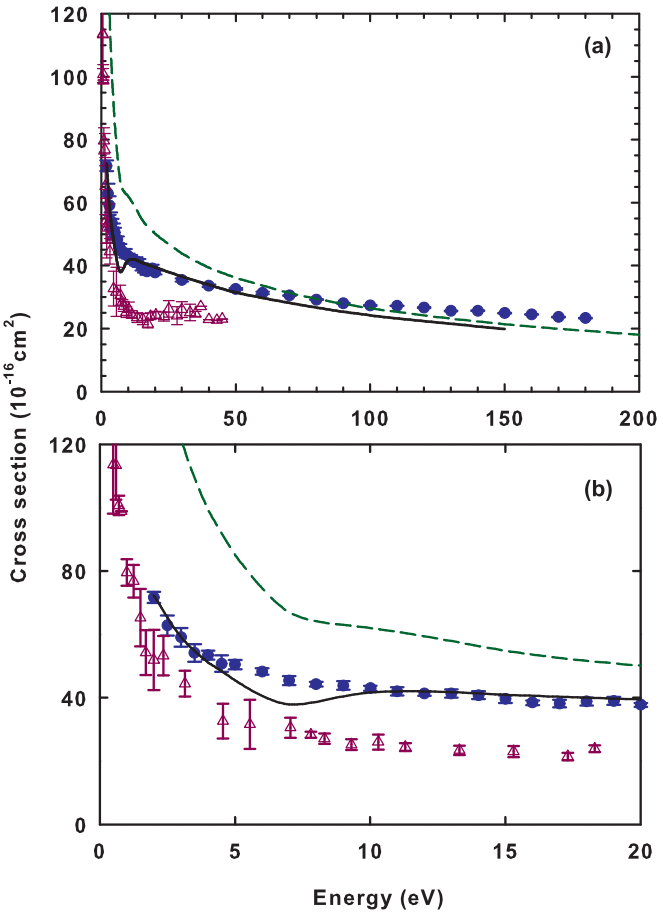

FIG. 1. (Color online) Present grand total cross-section measurements compared to other work. (a) Data over the full energy range. Blue circles are the present data and purple triangles are the work of Zecca *et al*. [17]. The dashed green line is the IAM-SCAR theory of Sanz *et al*. [18], including contributions from rotational excitations. The solid line is the same theory, but excluding the missing angles of the experiment, as given in Table I. (b) Low-energy range behavior. Symbols and lines are the same as for (a).

can be expected from a polar target. The similarity in the shape of the cross section between these two measurements indicates that most differences would be accounted for by the forward angle correction. A comparison with the adjusted IAM-SCAR theory of Sanz *et al*. is excellent at energies up to 80 eV, with the exception of a dip in the calculation between 3 and 10 eV. This is in the region immediately above the positronium formation threshold at 2.93 eV, and suggests that some improvement in the incorporation of this process into the theory may be warranted. At energies above 80 eV, there is little difference between the modified and original theory, suggesting that the role of the missing forward angles is only small. Despite this, there is some disagreement between the experiment and theory, up to about 25% at 180 eV, the highest experimental energy. The reason for this disagreement is unclear. Nonetheless, overall the agreement between the experiment and theory is very good, with the large difference between the full calculation and the experimental data at low energies demonstrating the importance of correctly accounting for the angular resolution of the experiment.

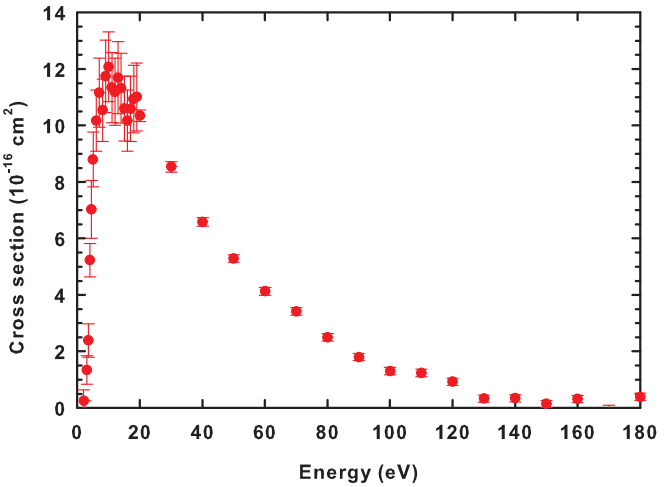

FIG. 2. (Color online) Present experimental data for the positronium formation cross section (•).

B. Partial total cross sections

The data in Fig. 2 are the first measurements of positronium formation from pyrimidine, and we note that no theory exists for this process. The cross section is typical of what is seen in other systems (see, for instance, [10,11]), rising sharply from threshold at 2.93 eV to a maximum of around 11 Å^2 at an energy of 10 eV and falling to zero at an energy of around 130 eV. The larger error bars for the lower-energy data are a consequence of a lower pressure used to make those measurements. This is due to the large total cross section, and results in a greater systematic error contribution from the pressure measurement.

The total elastic and total inelastic (including both electronic excitations and ionisation) cross sections are shown in

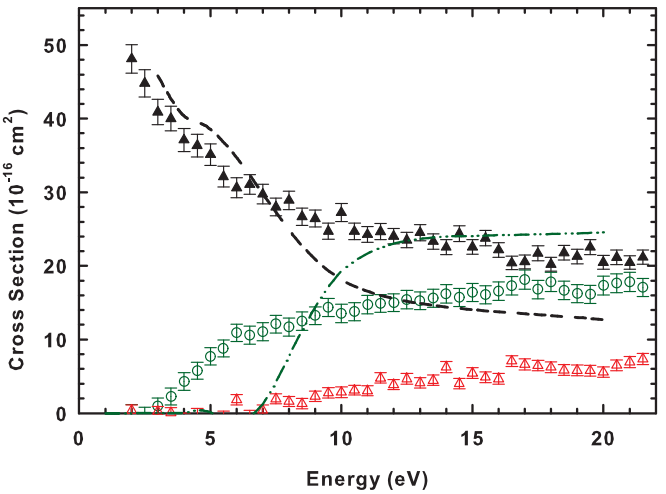

FIG. 3. (Color online) Total elastic and total inelastic cross sections. Solid triangles (black) are the experimental total elastic scattering data, compared to the calculation of Sanz *et al*. [18] (dashed black line). Open (red) triangles are the current total inelastic cross sections, including ionization and electronic excitation (see text), while the open (green) circles are the total inelastic summed with the positronium formation cross section, which is compared to the absorption part of the IAM-SCAR calculation from Sanz *et al*. [18] (chain line, green).

TABLE II. Present total scattering cross sections (10^{-16} cm^2).

Energy (eV)	Grand total	error	Ps formation	error	Energy (eV)	Total inelastic	error	Total elastic	error
2.00	71.66	1.73	0.25	0.39	2.00	0.39	0.74	48.11	1.90
2.50	62.84	3.17	0	0.55	2.50	0	0.74	44.81	1.84
3.00	59.07	2.98	1.34	0.50	3.00	0.24	0.70	40.90	1.71
3.50	54.18	2.74	2.39	0.60	3.50	0.05	0.71	40.00	1.69
4.00	53.47	1.36	5.23	0.59	4.00	0	0.71	37.11	1.57
4.50	50.79	2.58	7.03	1.03	4.50	0	0.72	36.35	1.55
5.00	50.51	1.48	8.79	0.97	5.00	0	0.67	35.11	1.46
6.00	48.28	1.03	10.17	1.08	5.50	0	0.66	32.12	1.38
7.00	45.44	1.41	11.16	1.22	6.00	1.82	0.70	30.62	1.35
8.00	44.33	0.74	10.54	1.11	6.50	0	0.71	31.06	1.33
9.00	43.90	1.36	11.74	1.28	7.00	0.40	0.69	29.76	1.31
10.00	43.02	0.79	12.08	1.24	7.50	1.94	0.70	28.00	1.20
11.00	42.06	1.31	11.34	1.24	8.00	1.59	0.69	28.91	1.25
12.00	41.34	0.80	11.19	1.19	8.50	1.30	0.69	26.68	1.18
13.00	41.35	1.28	11.70	1.28	9.00	2.30	0.69	26.44	1.17
14.00	40.81	1.27	11.32	1.24	9.50	2.75	0.70	24.70	1.10
15.00	39.60	1.16	10.60	1.15	10.00	2.85	0.74	27.24	1.22
16.00	38.49	0.74	10.17	1.09	10.50	3.12	0.66	24.67	1.12
17.00	38.21	1.19	10.59	1.16	11.00	3.03	0.69	24.25	1.08
18.00	38.85	1.21	10.94	1.20	11.50	4.77	0.69	24.66	1.09
19.00	39.04	1.22	11.01	1.20	12.00	3.88	0.67	24.02	1.05
20.00	37.81	0.61	10.35	0.21	12.50	4.68	0.71	23.49	1.05
30.00	35.46	0.51	8.54	0.18	13.00	4.10	0.68	24.53	1.10
40.00	33.63	0.42	6.58	0.15	13.50	4.45	0.69	23.30	1.05
50.00	32.60	0.25	5.29	0.14	14.00	6.25	0.75	22.53	1.01
60.00	31.35	0.39	4.13	0.14	14.50	4.00	0.68	24.38	1.08
70.00	30.54	0.13	3.41	0.13	15.00	5.43	0.72	22.56	1.01
80.00	29.20	0.12	2.50	0.13	15.50	4.88	0.71	23.78	1.06
90.00	28.05	0.12	1.80	0.13	16.00	4.67	0.71	22.16	1.00
100.00	27.36	0.12	1.30	0.13	16.50	7.07	0.73	20.37	0.92
110.00	27.24	0.12	1.24	0.13	17.00	6.61	0.75	20.53	0.93
120.00	26.67	0.11	0.92	0.13	17.50	6.45	0.72	21.70	1.00
130.00	25.59	0.11	0.33	0.13	18.00	6.23	0.72	20.20	0.92
140.00	25.66	0.11	0.34	0.13	18.50	5.83	0.73	21.77	0.98
150.00	24.91	0.11	0.14	0.13	19.00	5.79	0.72	21.27	0.98
160.00	24.49	0.11	0.31	0.13	19.50	5.76	0.74	22.52	1.02
170.00	23.67	0.10	0	0.13	20.00	5.55	0.72	20.46	0.94
180.00	23.29	0.10	0.39	0.13	20.50	6.48	0.73	21.14	0.97
					21.00	6.92	0.77	20.44	0.91
					21.50	7.35	0.74	21.16	0.98

Fig. 3, for energies up to 22 eV. The measured total elastic cross section is affected again by the forward angle resolution, as mentioned above and detailed in Table I. It also includes any contribution from rotational and vibrational excitation. When compared to the IAM-SCAR calculation for the elastic process, the shapes of the two cross sections are quite different. While the total inelastic cross section we measure cannot be directly compared to the theory, the absorption potential used in the IAM-SCAR method accounts for both the positronium formation and any inelastic processes, so the sum of these experimental cross sections is also shown in Fig. 3, compared to the corresponding partial cross section from the theory. In this case, we again see a substantial disagreement between the calculation and the measurement. Despite this observation, when it comes to the grand total cross section the effect of the overestimation of the inelastic cross section is canceled by the underestimation of the elastic cross section, and the experiment and theory are largely in agreement, except for the region between 3 and 10 eV. This lends weight to the previous suggestion that the discrepancy in the grand total cross section for those energies arises due to the difficulty of properly accounting for the positronium formation in the theoretical description of the problem. The experimental data for the grand total, total elastic, total inelastic, and positronium formation cross sections are presented in Table II.

C. Differential elastic cross section

In Fig. 4, we present our results for measurements of elastic differential cross sections, averaged over rotational and vibrational excitations. Energies range from 1 to 20 eV, and the data are compared to the IAM-SCAR and *R*-matrix

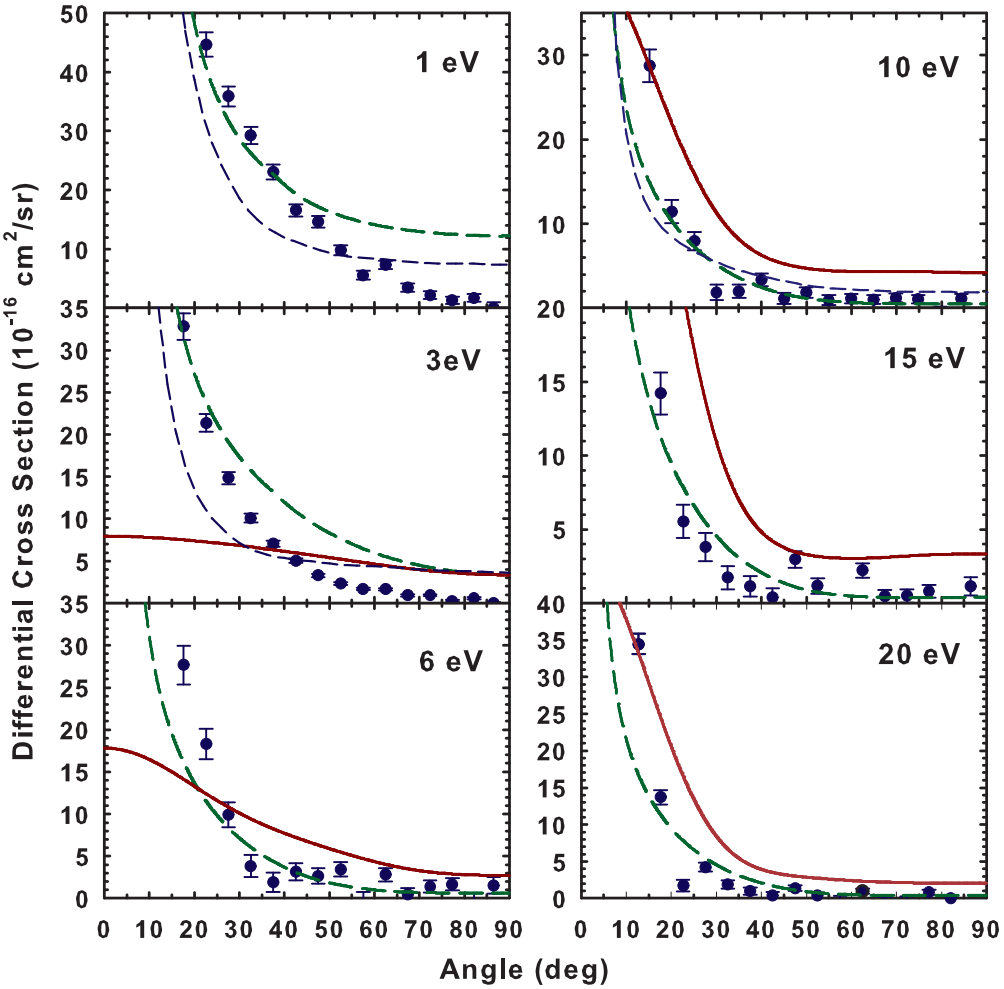

FIG. 4. (Color online) Elastic differential cross sections from 1 to 20 eV. The experimental data (solid circles) are compared to the IAM-SCAR (green dashed line) and *R*-matrix (short dashed line, blue) positron scattering calculations of Sanz *et al*. [18] and electron scattering data from Palihawadana *et al*. (see text) [15] (full red line).

calculations of Sanz *et al*. [18]. The *R*-matrix calculations using the close coupling (CC) approximation were chosen, as they are in the closest agreement with the current experimental results. A comparison is also made with the electron scattering Schwinger multichannel coupling (SMC) calculation published by Palihawadana *et al*. [15]. In the case of the electron scattering data, the experimental results from the paper were in good agreement with the SMC calculations, so only the theory is presented here in the interest of clarity. At the lowest energy, 1 eV, the experimental positron data are in good agreement with the IAM-SCAR calculation up to an angle of around 50°, while at higher angles the experiment lies below the calculation. The agreement with the *R*-matrix calculation is somewhat worse. At 3 eV, the experimental positron scattering cross section is smaller than the IAM-SCAR calculation for all angles measured, although it appears that the overall agreement is somewhat improved compared to the 1-eV case, with a smaller discrepancy at the larger scattering angles. The *R*-matrix calculation again compares less favorably to the experiment, although the comparison appears to be improving. There is a large discrepancy between the electron and positron data at this energy, with a much smaller degree of forward peaking in the electron scattering case. It was suggested by Palihawadana *et al*. that dynamic processes not related to the dipole moment and polarizability might be the cause for the unexpectedly "flat" cross section in the electron scattering case, although at lower angles the inclusion of dipole effects in the calculation (not accounted for in [15]) would result in the expected sharp rise. Given the differences between positron and electron scattering in this case, it may be that electron correlations or even negative ion resonances are the cause of the differences observed here. This trend continues through to 6 eV, with the agreement with the IAM-SCAR calculation improved, albeit with some discrepancies at the most forward angles, as well as an improved agreement between the electron and positron scattering cases, although noting similar differences as observed previously in the forward angles. At 10 eV, both the positron calculations and experiment are in good agreement, with perhaps the IAM-SCAR theory more closely in line with the experiment than the *R*-matrix calculation at this energy. The positron data now lie below the electron scattering results at this energy, for all angles. At 15 and 20 eV, the comparison between the positron and electron scattering cases is much the same. The agreement between the present data and

TABLE III. Present differential elastic scattering cross sections (10^{-16} cm^{2}str^{-1}).

Angle	1 eV	Error	3 eV	Error	6 eV	Error	15 eV	Error	20 eV	Error	Angle	10 eV	Error
12.5	–	–	–	–	–	–	–	–	34.47	1.37	15	28.73	1.92
17.5	–	–	32.80	1.60	27.67	2.27	14.21	1.43	13.71	0.98	20	11.45	1.38
22.5	44.62	2.06	21.39	1.05	18.29	1.81	5.54	1.12	1.71	0.75	25	7.95	1.11
27.5	35.87	1.68	14.84	0.74	9.91	1.48	3.81	0.94	4.25	0.62	30	1.88	0.93
32.5	29.24	1.44	10.10	0.51	3.83	1.29	1.75	0.79	1.86	0.54	35	1.99	0.80
37.5	23.05	1.23	7.01	0.37	1.91	1.14	1.15	0.69	0.96	0.49	40	3.36	0.74
42.5	16.56	1.05	5.04	0.28	3.18	1.03	0.39	0.63	0.38	0.44	45	1.16	0.66
47.5	14.67	0.97	3.30	0.21	2.66	0.93	2.97	0.58	1.39	0.40	50	1.83	0.60
52.5	9.81	0.84	2.32	0.16	3.44	0.86	1.16	0.53	0.38	0.37	55	0.93	0.57
57.5	5.58	0.77	1.70	0.14	0	0.84	0	0.51	0	0.36	60	1.14	0.55
62.5	7.31	0.74	1.63	0.13	2.81	0.79	2.22	0.48	0.98	0.34	65	1.01	0.53
68	3.47	0.69	0.93	0.11	0.46	0.76	0.46	0.46	0	0.32	70	1.18	0.52
72	2.17	0.66	0.95	0.11	1.40	0.74	0.49	0.46	0	0.31	75	1.08	0.49
77	1.31	0.64	0.25	0.10	1.64	0.71	0.81	0.44	0.82	0.31	80	0	0.50
82	1.74	0.67	0.58	0.11	0	0.73	0	0.46	0.00	0.31	84.5	1.11	0.54
86.5	0.03	0.92	0.02	0.14	1.54	0.97	1.15	0.61	0.36	0.42	–	–	–

the IAM-SCAR theory for positron scattering is excellent at these two energies. All the behaviors evident in the measurements of the differential cross section are consistent with the physico-chemical properties of pyrimidine outlined in the Introduction. A summary of the experimental data presented here is given in Table III.

IV. CONCLUSION

This paper presents measurements of cross sections for positron scattering from pyrimidine. The grand total cross section is in reasonable agreement with previous experimental data [17], when the differing angular discriminations of the two experiments is taken into consideration. When comparing our grand total cross sections to the only available theoretical results for this molecule [18], we find good agreement at energies up to about 80 eV, when the experimental angular resolution is taken into account. At higher energies, there is a disagreement of up to 25% in magnitude between the experiment and theory, which is unaccounted for. The comparison between the theory and experiment for the elastic differential cross section also reflects this, with a good agreement at energies of 10 eV and above with both the IAM-SCAR and *R*-matrix calculations, and some discrepancies for lower energies, which is to be expected given the previously suggested limits on the validity of that approach at low energies. This suggests that at least a part of the disagreement in the total cross sections is explained by the angular resolution limitation of the experimental procedure, while there also appears to be some inadequacies in the theoretical approach. A comparison with electron scattering data shows that the low-energy DCSs are quite different between positron and electron scattering, demonstrating that more than a simple dipole scattering approach is required to accurately describe the scattering process. Positronium formation cross sections, total elastic, and total inelastic cross sections were also measured. The partitioning of the cross section at this level is quite different between the experiment and theory, complicated by the difficulty of accurately incorporating positronium formation into the theoretical description of the process. It is clear, however, from considering both these experiments and the theory of Sanz *et al.* [18] that the dipole moment and dipole polarizability of pyrimidine both play critical roles in the scattering dynamics of this system.

Nonetheless, it is demonstrated here that there is reasonable agreement between the experiment and theory for the process of positron scattering from pyrimidine, certainly at the total cross-section level. As part of an ongoing investigation into positron interactions with biologically relevant molecules, the present work represents a significant step in building a reliable database of cross sections that may be used in simulations of positron thermalization and transport within the body.

ACKNOWLEDGMENTS

The authors would like to acknowledge funding from the ARC Centres of Excellence program for their support of this work, as well as the excellent technical support of Steve Battisson and Ross Tranter. We also gratefully acknowledge the provision of theoretical results in advance of publication by A. G. Sanz, M. C. Fuss, F. Blanco, Z. Mašín, J. D. Gorfinkiel, and G. García, especially for their willingness to provide data reflecting the angular resolution limitations of the experiments presented here.

[1] G. G. Gomez-Tejedor and M. C. Fuss, *Radiation Damage in Biomolecular Systems* (Springer, Berlin, 2012).

[2] S. Jaini and E. Dadachova, Semin. Nucl. Med. **42**, 185 (2012).

[3] A. G. Sanz, M. C. Fuss, A. Munoz, F. Blanco, P. Limao-Vieira, M. J. Brunger, S. J. Buckman, and G. Garcia, Int. J. Radiat. Biol. **88**, 71 (2012).

[4] A. Munoz, F. Blanco, G. Garcia, P. A. Thorn, M. J. Brunger, J. P. Sullivan, and S. J. Buckman, Int. J. Mass Spectrom. **277**, 175 (2008).
[5] J. Baro, J. Sempan, J. M. Fernandez-Varea, and F. Salvat, Nucl. Instrum. Methods B **100**, 31 (1995).
[6] S. Agostinelli *et al.*, Nucl. Instrum. Methods A **506**, 250 (2003).
[7] M. J. Brunger, S. J. Buckman, and A. Zecca, J. Phys.: Conf. Ser. **194**, 012034 (2009).
[8] E. Surdutovich, G. Setzler, W. E. Kauppila, S. J. Rehse, and T. S. Stein, Phys. Rev. A **77**, 054701 (2008).
[9] C. Makochekanwa, A. Bankovic, W. Tattersall, A. Jones, P. Caradonna, D. S. Slaughter, K. Nixon, M. J. Brunger, Z. Petrovic, J. P. Sullivan, and S. J. Buckman, New J. Phys. **11**, 103036 (2009).
[10] L. Chiari, E. Anderson, W. Tattersall, J. R. Machacek, P. Palihawadana, C. Makochekanwa, J. P. Sullivan, G. Garcia, F. Blanco, R. P. McEachran, M. J. Brunger, and S. J. Buckman, J. Chem. Phys. **138**, 074301 (2013).
[11] L. Chiari, P. Palihawadana, J. R. Machacek, C. Makochekanwa, G. Garcia, F. Blanco, R. P. McEachran, M. J. Brunger, S. J. Buckman, and J. P. Sullivan, J. Chem. Phys. **138**, 074302 (2013).
[12] P. L. Levesque, M. Michaud, and L. Sanche, J. Chem. Phys. **122**, 094701 (2005).
[13] A. Hinchliffe and H. J. S. Machado, Int. J. Mol. Sci. **1**, 8 (2000).
[14] G. L. Blackman, R. D. Brown, and F. R. Burden, J. Mol. Spectrosc. **35**, 444 (1970).
[15] P. Palihawadana, J. P. Sullivan, M. Brunger, C. Winstead, V. McKoy, G. Garcia, F. Blanco, and S. J. Buckman, Phys. Rev. A **84**, 062702 (2011).
[16] P. Palihawadana, J. P. Sullivan, S. J. Buckman, and M. J. Brunger, J. Chem. Phys. **137**, 204307 (2012).
[17] A. Zecca, L. Chiari, G. Garcia, F. Blanco, E. Trainotti, and M. J. Brunger, J. Phys. B **43**, 215204 (2010).
[18] A. G. Sanz, M. C. Fuss, F. Blanco, Z. Mašín, J. D. Gorfinkiel, M. J. Brunger and G. Garcia (unpublished).
[19] S. J. Gilbert, C. Kurz, R. G. Greaves, and C. M. Surko, Appl. Phys. Lett. **70**, 1944 (1997).
[20] J. P. Sullivan, A. Jones, P. Caradonna, C. Makochekanwa, and S. J. Buckman, Rev. Sci. Instrum. **79**, 113105 (2008).
[21] J. P. Sullivan, S. J. Gilbert, J. P. Marler, R. G. Greaves, S. J. Buckman, and C. M. Surko, Phys. Rev. A **66**, 042708 (2002).
[22] J. P. Sullivan, C. Makochekanwa, A. Jones, P. Caradonna, D. S. Slaughter, J. Machacek, R. P. McEachran, D. W. Mueller, and S. J. Buckman, J. Phys. B **44**, 035201 (2011).